Nitrogen-Doped Carbon Dots/TiO2 Nanoparticle Composites for Photoelectrochemical Water Oxidation

Hui Luo, Stoichko Dimitrov, Matyas Daboczi, Ji-Seon Kim, Qian Guo, Yuanxing Fang, Marc Antoine Stoeckel, Paolo Samori, Oliver Fenwick, Ana Belen Jorge Sobrido, et al.

Nitrogen-doped Carbon Dots/TiO_2 Nanoparticle Composites for Photoelectrochemical Water Oxidation

*Hui Luo,[a,g] Stoichko Dimitrov,[b,c] Matyas Daboczi,[d] Ji-Seon Kim,[d] Qian Guo,[a] Yuanxing Fang,[e] Marc-Antoine Stoeckel,[f] Paolo Samorì,[f] Oliver Fenwick,[a] Ana Belen Jorge Sobrido,[a] Xinchen Wang [e] and Maria-Magdalena Titirici [a,g] **

a. School of Engineering and Materials Science, Queen Mary University of London, Mile End Road, E1 4NS, London, UK

b. SPECIFIC, College of Engineering, Swansea University SA2 7AX, Swansea, UK

c. School of Biological and Chemical Sciences, Queen Mary University of London, Mile End Road, E1 4NS, London, UK

d. Department of Physics and Centre for Plastic Electronics, Imperial College London, South Kensington Campus, SW7 2AZ, London, UK

e. State Key Laboratory of Photocatalysis on Energy and Environment, College of Chemistry, Fuzhou University, Fuzhou, 350116 P. R. China

f. Université de Strasbourg, CNRS, ISIS, 8, allée Gaspard Monge, 67000, Strasbourg, France

g. Department of Chemical Engineering, Imperial College London, South Kensington Campus, SW7 2AZ, London, UK

Corresponding author e-mail: m.titirici@imperial.ac.uk

KEYWORDS: Carbon dots, Photoelectrocatalysis, Heterojunction, Charge transfer, Band structure

ABSTRACT

Carbon dots on photoactive semiconductor nanomaterials have represented an effective strategy for enhancing their photoelectrochemical (PEC) activity. By carefully designing and manipulating carbon dots/support composite, a high photocurrent could be obtained. Currently, there is not much fundamental understanding of how the interaction between such materials can facilitate the reaction process. This hinders the wide applicability in PEC devices. To address this need of improving the fundamental understanding of carbon dots/semiconductor nanocomposite, we have taken the TiO_2 case as a model semiconductor system with nitrogen-doped carbon dots (NCDs). We present here with in-depth investigation of the structural hybridization and energy transitions in the NCDs/TiO_2 photoelectrode *via* high-resolution scanning transmission microscopy (HR-STEM), electron energy loss spectroscopy (EELS), UV-Vis absorption, electrochemical impedance spectroscopy (EIS), Mott-Schottky (M-S), time-correlated single photon counting (TCSPC) and ultra-violet photoelectron spectroscopy (UPS), which shed some light on the charge transfer process at the carbon dots and TiO_2 interface. We show that N doping in carbon dots can

effectively prolong the carrier lifetime, and the hybridisation of NCDs and TiO_2 is able not only to extend TiO_2 light response into the visible range but also to form heterojunction at the NCDs/TiO_2 interface with properly aligned band structure that allows a spatial separation of the charges. This work is arguably the first to report the direct probing of the band positions of carbon dots-TiO_2 nanoparticle composite in a PEC system for understanding the energy transfer mechanism, demonstrating the favourable role of NCDs in the photocurrent response of TiO_2 for water oxidation process. This study reveals the importance of combining structural, photophysical and electrochemical experiments to develop a comprehensive understanding of the nanoscale charge transfer processes between the carbon dots and their catalyst supports.

1. Introduction

Photoelectrochemical (PEC) water splitting for hydrogen and oxygen production represents a promising technology for the conversion of solar energy to clean and renewable chemical fuels. Since the first report on PEC water splitting in 1972 using TiO_2 photoelectrode,[1] many efforts have been made to improving the light conversion efficiency. To achieve the overall reaction, the water oxidation happening at photoanode is a crucial step as it requires higher energy input. Several approaches have been reported in the literature to improve the performance of the photoanode materials, such as heteroatom doping,[2] nanostructring[3] *etc*. Among those, constructing heterojunctions in nanoscale materials like CdS/TiO_2,[4–8] graphene/TiO_2,[9,10] carbon dots/TiO_2[11–15] has been demonstrated to be an effective strategy. The enhanced PEC performance of the CdS/TiO_2 system is assigned to the electric-field-assisted charge transport at the interface with matched band alignments, which can improve the charge separation and prolong the photo-induced carrier lifetime. In the case of graphene or reduced graphene oxide, those 2D and zero bandgap

materials serve as electron mediator when coupled with TiO_2, allowing an accelerated electron migration at the interface.

Carbon dots with size less than 10 nm have been demonstrated to act as photosensitizers for enhancing the performance of heterogeneous photocatalysts, due to their adjustable band potentials, excellent and tunable light-harvesting ability, and electron transfer efficiency.[12,16–20] When doped with nitrogen,[13,21,22] carbon dots usually show an enhanced activity towards photo-driven reactions both experimentally and theoretically.[23,24] Accordingly, the utilisation of nitrogen-doped carbon dots (NCDs) photosensitizers to facilitate PEC reactions started to attract attention.[13,21,25] However, owing to the complexity of NCDs compare to CdS and graphene in terms of chemical structure and energy states, the mechanism of NCDs in improving the PEC performance is still not well understood and explained.[12,17,26] Previous studies have indirectly demonstrated that the electronic coupling between the π states of the CDs and the conduction band of TiO_2 can form heterojunctions and impart the system for visible light absorption. The resulting heterojunction can efficiently separate the photo-generated electrons and holes, resulting in a lower recombination rate and a higher PEC activity.[14] Those effects can be greatly influenced by the intrinsic properties of CDs. For instance, the graphitisation degree can affect the charge transfer process,[27] the different N doping configuration (amines, amides, pyridinic, quaternary, N-oxides, etc.) can govern the light-harvesting ability,[28] while the functionality would determine the interaction with supporting materials.[16,29] Hence, it is of vital importance to develop a deeper understanding of the nanostructure of CDs and their interaction with the semiconductor materials and gain further insights on the dynamics of the charge exchange process at the materials interface.

In this paper, we exploit a broad arsenal of complementary advanced characterisation technique to understand the morphology, structure, optical and electrochemical properties of chitosan derived

NCDs at a fundamental level. Such studies reveal that N doping can effectively prolong the photo-induced carrier lifetime. A photoanode was prepared by decorating the as-synthesized NCDs onto a TiO_2 mesoporous film, which is used as a model semiconductor material to study the NCDs/semiconductor interaction. A detailed structural and PEC analysis showed that the nanoparticle composite possesses an improved visible light response as well as charge separation/transport ability, which resulted in a higher photocurrent value. In-depth characterisation of the NCD/TiO_2 nanocomposite by methods such as Mott-Schottky analysis, photoelectron spectroscopy in air, Kelvin probe and ultra-violet photoelectron spectroscopy was employed to evaluate the energy levels. Combined with electrochemical impedance spectroscopy (EIS) and in-situ photoluminescence quenching by time-correlated single photon counting (TCSPC), we present here the detailed mechanism for the interfacial charge transfer process.

2. Results and discussion

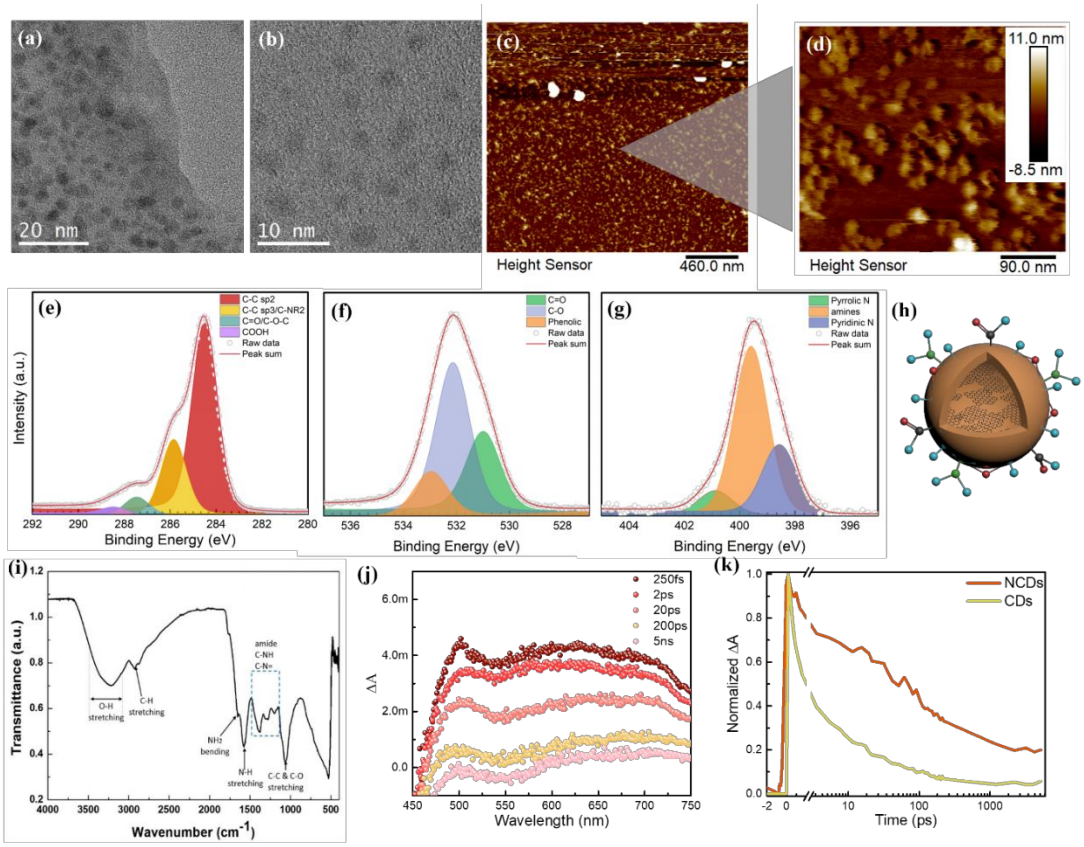

Figure 1 Structural features of as-prepared NCDs: TEM (a) and HR-TEM (b) images; (c) an overview AFM image on mica substrate (Z scale -6.0 to 7.9 nm) and (d) high-resolution scanned image; XPS spectra: (e) C 1s, (f) O 1s, (g) N 1s and corresponding FTIR (i) spectrum; (h) a schematic structure based on the characterizations (atoms in red: O, green: N and blue: H); (j) fs-TAS spectra at different time decays and (k) normalized fs-TAS kinetics of NCDs and non-doped CDs measured at 500 nm (excitation wavelength: 375 nm).

NCDs were synthesized by solvothermal carbonisation of chitosan in ethanol solvent (4% w/v). Several works on using chitosan to produce NCDs have been reported earlier.[30–32] Under mild conditions (HTC with 180 °C), the carbonisation and functionalisation will take place through chitosan dehydration, leading to the formation of NCDs. As illustrated in **Figure S1**, the precursor molecules go through decomposition to HMF and ammonia. The HMF molecule then go through ring opening to react with ammonia and form aminopentanals. Intermolecular condensation would occur at this stage in these intermediates. Pyridines would form from the reaction between amino groups and aldehyde, while the reaction between amino and keto groups results in the formation of pyrroles. Some amines remain free from reacting with other groups.[33] These functionalities are later identified in the structure of NCDs.

Figure 1(a, b) shows the transmission electron microscopy (TEM) images of NCDs with spherical morphologies. The atomic force microscopy (AFM) images of the NCDs (**Figure 1c, d**) further prove that the sizes of those NCDs are uniformly distributed. The CDs are ~ 2-8 nm in height, values obtained from cross-sectional topographic measurements, taken into account the broadening effect due to the finite size of the tip.

To analyse the structure of the carbon core, the output of XRD and Raman spectroscopy techniques were compared. The X-ray diffraction (XRD) pattern (**Figure S2a**) displays a broad

peak centred at 21°, which has been demonstrated to be amorphous with turbostratic structure in our previous study.[31] In theory, XRD involves X-rays interacting with electrons to reveal the reciprocal space of crystalline lattice by diffraction, which does not give sufficient structural information of packed carbon dots due to the less ordered structure. In this regard, Raman spectroscopy uses long wavelength radiation and interacts with atoms, molecules or ions, which can reveal the vibration frequencies of the system by scattering, providing information about the chemical environments. Hence here Raman spectroscopy was carried out for the surface characterisation of partially ordered carbon materials.[34] **Figure S2b** shows the Raman spectra (λ = 633 nm) of the NCDs. Two peaks centred at 1382 cm^{-1} and 1574 cm^{-1} can be seen, representing the characteristic D and G bands for carbon materials, respectively, indicating a semi-crystalline structure of the NCDs. The spectra show a significant level of noise-to-signal ratio, due to the highly fluorescent background removal.

The X-ray photoelectron spectroscopy (XPS) spectra are shown in **Figure 1(e, f, g)**. They reveal that the amine groups from chitosan are mentained on the surface of NCDs, and the carbon, oxygen, nitrogen contents have been calculated to be 75.8%, 28.2% and 5.8%, respectively. Three types of nitrogen species can be found in the material, which are pyridinic N (26%), amine groups (64%) and pyrrolic N (10%), existing both on the surface as functional groups and incorporated inside the core structure. It has been reported that different N-motifs show different charge transportation properties, which will be beneficial for the PEC properties.[28] The Fourier transform infrared (FTIR) spectrum in **Figure 1(i)** also confirms the existence of amine groups in the NCDs, with NH_2 bending at 1648 cm^{-1} and N-H stretching at 1576 cm^{-1}. The peaks between 1151 and 1484 cm^{-1} are assigned to C-NH and C-N= amide groups.[35,36] A schematic profile representing the structure of NCDs is shown in **Figure 1h**.

The optical properties of the NCDs are analyzed by UV-Vis absorption and photoluminescence. As shown in **Figure S3a**, the UV-Vis absorption spectrum of NCD solution exhibits strong, broad light absorption in the ultraviolet range, with an absorption peak at 270 nm, which tails off in the visible region. The 270 nm absorption peak is due to the $\pi \rightarrow \pi^*$ transition, while the visible light absorption comes from $n \rightarrow \pi^*$ transition.[37,38] The visible light response of the synthesized NCDs is advantageous for use as a photosensitizer.[14] In **Figure S3b**, excitation-dependent emission was observed in the blue-green light region depending on the excitation wavelength, indicating easy access to the electronic states ($n-\pi^*, \pi-\pi^*$).[39] These interesting optical properties grant the NCDs with potential applications in hybrid PEC design. Photoluminescence quantum yield (Φ) of NCDs was calculated to be 8.7% referenced by quinine sulphate (QS).[40]

Our previous work has shown that the NCDs derived from chitosan are capable of generating photocurrents under visible light irradiation, akin to the electronic structure of n-type semiconductor, and the excited states of carbon dots upon interaction with light govern the photo-induced activity.[31] To investigate the nature of stable surface paramagnetic defects, EPR measurements were performed on NCD powder at room temperature in dark condition. In **Figure S4**, the sharp isotropic EPR signals centred at g_{iso}=2.0035 is expected to come from the presence of carbon centred radical species present on the NCD surface, which could act as active sites for redox reactions.

The excited state photophysical properties of NCDs were investigated by mean of femtosecond transient absorption spectroscopy (fs-TAS) which reveals that upon 375 nm photoexcitation, NCDs gave rise to differential absorption signals that are spanning over the visible range from 450-750 nm on a ps timescale (**Figure 1j**). Features are centred near 500 nm and 625 nm, similar to previously reported spectra of CDs.[27,37] The features showed up at shorter and longer

wavelengthes are possibly assigned to core and surface states of CDs, respectively. This behaviour is akin to that observed for graphitic carbon dots.[27,41] The decay lifetime kinetics at 500 nm were fitted using a bi-exponential function into short (2.17 ps, 39%) and long (138.97 ps, 61%) lived components. The extracted excitons lifetimes have been found being longer than any other photosensitising materials reported to date.[42,43] The comparison of the decay profile of NCDs with that of non-doped CDs in **Figure 1k** reveals that doping with N has largely prolonged the exciton lifetime, being beneficial for the PEC process. This might be a result of N doping reducing π-connections between sp^2 domains, suppressing the interlayer non-radiative energy dissipation,[21] and serve as electron donor to effectively scavenge holes to extend the lifetime of photogenerated electrons.[27] Here we have demonstrated for the first time clear evidence and explanation of the positive effect of N doping in carbon dots for the application as efficient photosensitizers. We have applied the prepared NCDs to TiO_2, which is an ideal model semiconductor to study the effect of the NCDs in the recombination rate of the photogenerated charge carriers in a PEC system. Compared to inorganic semiconducting quantum dots, carbon dots consist of mostly sp^2 carbon, which helps the formation of a charge-transfer complex with TiO_2 and thus resulting in more efficient absorption and charge separation.[44]

The TiO_2 thin film is fabricated by spin-coating a commercially available mesoporous titania paste onto fluorine-doped tin oxide (FTO) coated glass substrate. To gain insight into the morphology of the TiO_2 film, we performed SEM top-view and cross-section imaging of the NCDs/TiO_2 film, with representative images portrayed in **Figure S5**. No major aggregation of the nanoparticles can be observed. The thickness of the film was measured to be ~ 1 μm (from the SEM cross-section), considered adequate to provide good charge carrier generation and collection ability.[45] Brunauer-Emmett-Teller (BET) measurements showed that the TiO_2 has a specific

surface area of 110 m^2/g, higher than the commercial P25 (49 m^2/g). The mesoporosity, as seen from the SEM top view image guarantees sufficient light absorption and is also beneficial for anchoring the NCDs on its surface and inside the TiO_2 films, providing more active sites for reactions.[14]

Figure S6 displays the XRD patterns of the TiO_2 and NCDs/TiO_2 films. The dominant peak in both samples are assigned to the (101) facet of anatase phase, which is considered to be the most stable structure in anatase TiO_2.[46] The diffraction patterns of NCDs/TiO_2 are in good match with that of the TiO_2 which contains mostly anatase phase with small amount of rutile (JCPDS 01-084-1286, 01-073-2224), indicating that the deposition of NCDs does not cause any obvious changes in TiO_2 crystallinity.[47]

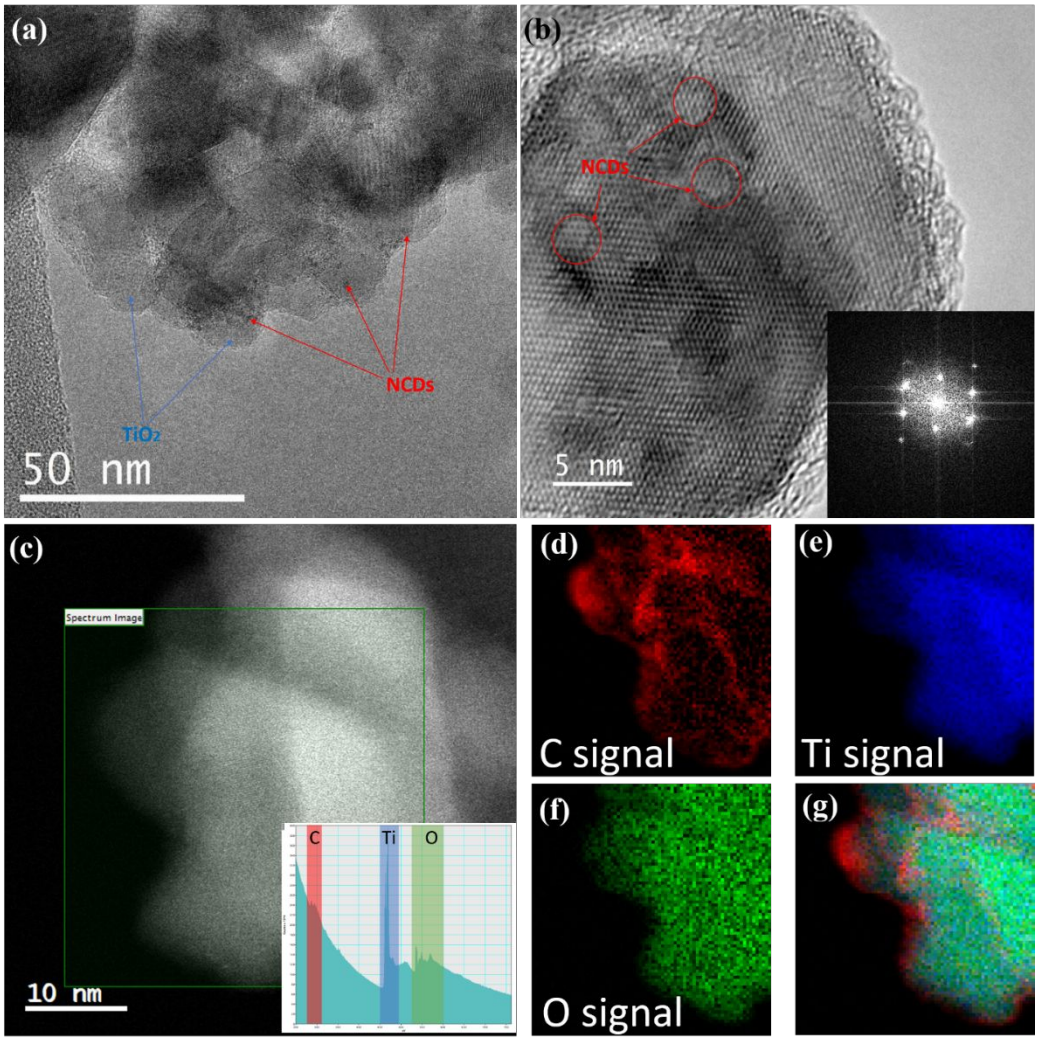

Figure 2 TEM (a) and HR-TEM (b) of NCDs/TiO_2 (insert is the FFT patterns); (c) HAADF image of NCDs/TiO_2 and corresponding EELS spectra (inserted). The single element maps derived from the spectra: (d) C signal, (e) Ti signal, (f) O signal and (g) colour mix (red: C, blue: Ti, green: O).

TEM and HR-TEM were used to investigate the morphologies of the NCDs/TiO_2 nanoparticles further. TEM image (**Figure 2a**) of the prepared NCDs/TiO_2 nanoparticles taken at low-magnification shows some dark spots dispersed on the surface of the TiO_2, revealing that the NCDs have been effectively deposited onto TiO_2. In the HR-TEM images, the NCDs became less obvious, leaving only contract differences due to the small particle size and less crystallined nature

of the NCDs compared to TiO_2 nanoparticles, as determined by TEM and XRD (**Figure 1 and S2**). The observed lattice spacing of 0.35 nm for TiO_2 nanoparticles correspond to the (101) plane of anatase TiO_2, as can be seen from XRD patterns in **Figure S6**. To further resolve the presence of NCDs, high-angle annular dark-field image (HAADF) was taken on several TiO_2 nanoparticles under high magnification. As seen in **Figure 2c**, NCDs are difficult to discern through the dark-field image due to the light element contrast. At the same area electron energy loss spectra (EELS) was scanned. It is known that EELS is better than EDS at detecting light elements due to the smaller energy window. Here we chose to look at 250 - 750 eV, which contains the characteristic spectra of carbon, nitrogen, titanium and oxygen, as illustrated in **Figure 2c** inserted. The spectra of C, Ti and O are very distinctive, while no signal can be seen from N, probably due to the low nitrogen amount in the NCDs (N 5.8%) also loaded in small amounts on the TiO_2 (~2.4% calculated from the mass loss in **Figure S7**). The EELS maps of individual elements along with the colour mix are shown in **Figure 2(d-g)**. The mapping of the NCDs on TiO_2 infers the heterostructure formation, which may promote the charge separation within the hybrid system, corroborating the improved PEC activity.[48]

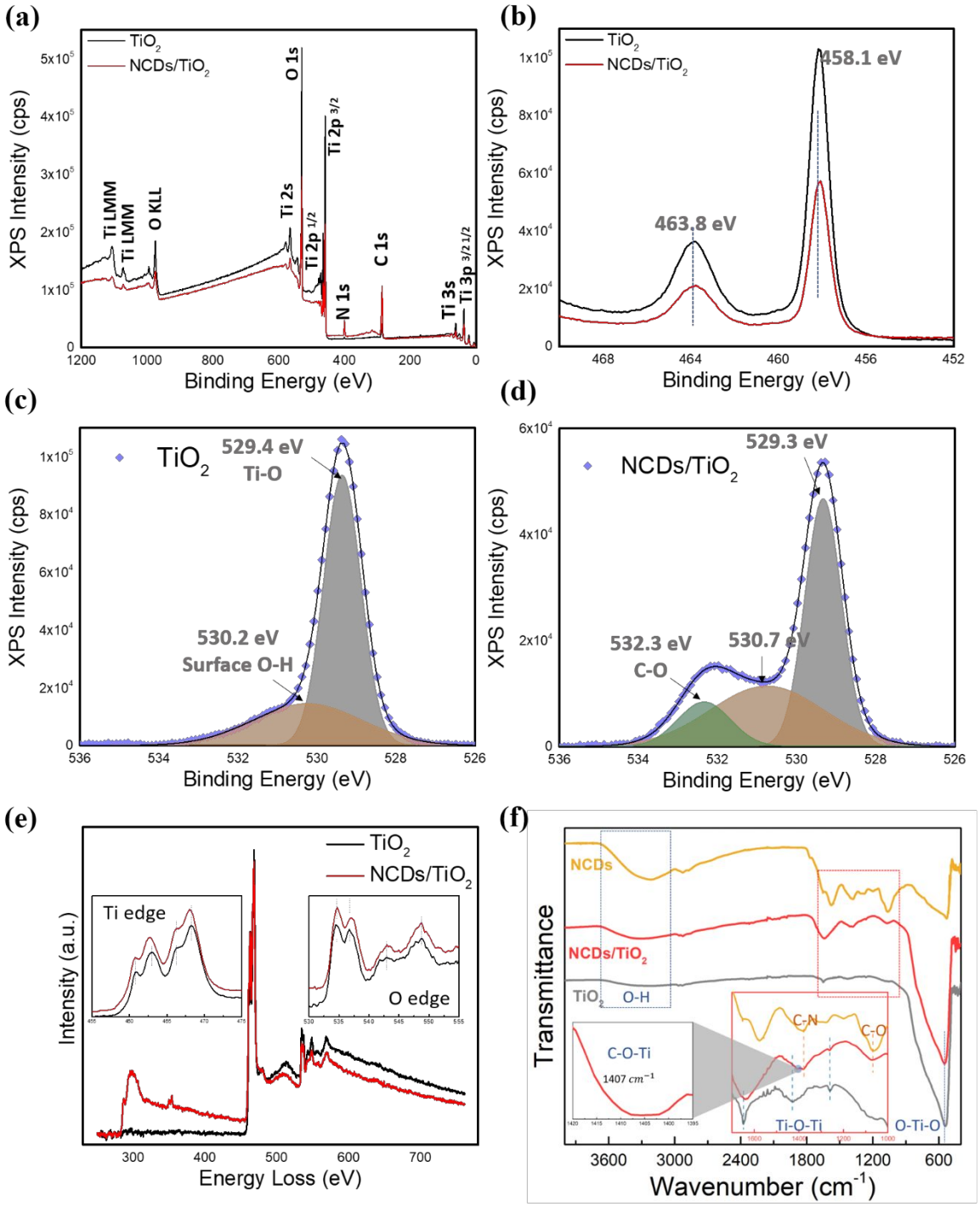

Figure 3 Comparison of XPS survey spectra (a) and Ti 2p high-resolution spectra (b) of the TiO_2 and NCDs/TiO_2 films; O 1s spectra of (c) TiO_2 and (d) NCDs/TiO_2. (e) EELS spectra of TiO_2 (black) and NCDs/TiO_2 (red) and (f) FTIR signals.

The chemical structure of the NCDs/TiO_2 was analysed by XPS. Compared to the pristine TiO_2, the survey spectrum (**Figure 3a**) of NCDs/TiO_2 showed higher intensity in C and N peaks, which originates from the NCDs. The deconvoluted high-resolution signals of Ti 2p (**Figure 3b**) show no shift in the binding energy, suggesting that there is no disruption of the TiO_2 structure after anchoring of the NCDs. The peaks at 458.1 eV and 463.8 eV are orginated from the pair of Ti $2p_{3/2}$ and Ti $2p_{1/2}$, respectively, assigned to the Ti^{4+} sp peaks of TiO_2. **Figure 3c** shows the O 1s spectra of TiO_2, in which the peaks at 529.4 eV and 530.2 eV arise from Ti-O and surface O-H groups in TiO_2, respectively.[49] After depositing of NCDs, the surface O-H peak shifted towards higher binding energy, suggesting that the chemical environment has been changed due to the interaction between the TiO_2 and NCDs and the formation of the Ti-O-C bond.[11] The O 1s spectrum also showed a peak at 532.3 eV corresponding to C-O bonds, which is also present in the O 1s spectra of NCDs (**Figure 1f**). The energy shift can also be observed in high-resolution EELS spectra at Ti and O edges after depositing NCDs (**Figure 3e**), suggesting a chemical environment change around surface Ti and O atoms.[50,51]

The formation of NCDs/TiO_2 hybrid has been further confirmed by FTIR analysis. **Figure 3f** shows that the spectra of NCDs/TiO_2 display typical vibration of O-Ti-O at 550 cm^{-1}, as well as C-N, C-O stretching at 1378 and 1067 cm^{-1}, confirming the presence of NCDs in the hybrid sample. A new absorption peak arises between the Ti-O-Ti and C-N bond at 1407 cm^{-1}, which is possible through the C-O-Ti bond formation.[52] Based on the above results, it can be concluded that the NCDs are loaded on the TiO_2 *via* chemical absorption.

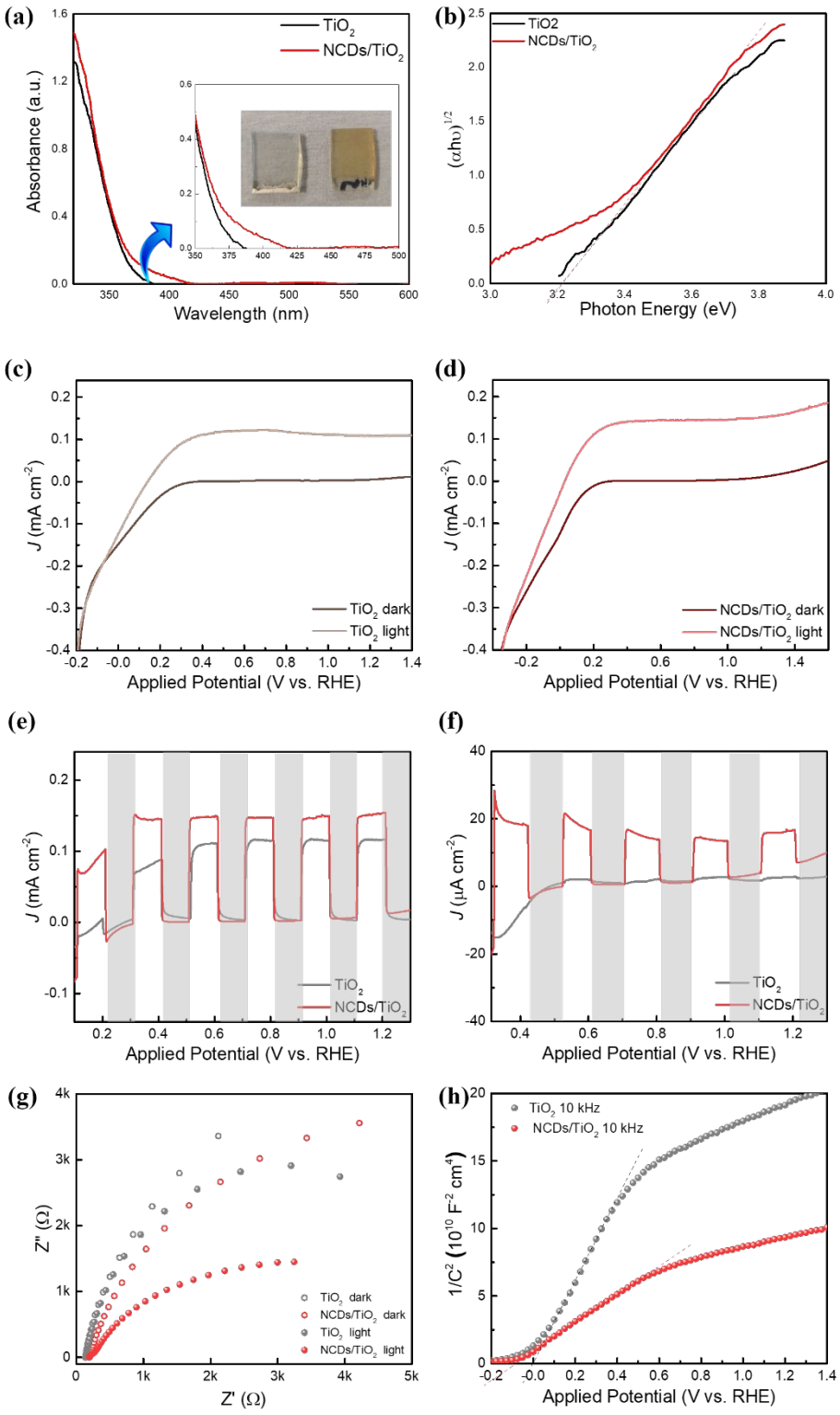

Figure 4 optoelectronic properties of TiO_2 and NCDs/TiO_2 films: (a) UV-Vis absorption (inserted are the digital pictures of the films: left: TiO_2, right: NCDs/TiO_2); (b) tauc plot of TiO_2 and

NCDs/TiO_2 with indirect band gap; LSV curves of (c) TiO_2 and (d) NCDs/TiO_2 under dark and light conditions; the chopped photocurrent response of the two samples under (e) full spectrum and (f) visible light ($\lambda > 420$ nm) illumination; (g) EIS Nyquist plots under simulated solar light illumination (100 kHz – 0.1 Hz, 0.3V vs. RHE, 100 mW cm^{-2}) and (h) Mott-Schottky plots with 10 kHz frequency under dark condition at equilibrium.

Light absorption is one of the essential factors determining the PEC performance of electrode materials. UV-Vis-NIR spectroscopy is employed to characterise the optical properties of the TiO_2 films and their respective NCD hybrids. As shown in **Figure 4a**, pure TiO_2 show no absorption above 385 nm owing to the intrinsic wide band gap of anatase TiO_2 (3.2 eV). Compared to the pristine TiO_2 film, the NCD decorated films show enhanced visible light absorption tails up to 425 nm for NCDs/TiO_2. Therefore, the presence of NCDs plays a critical role in boosting the visible light absorption of the composites, which is important for visible-light-driven photoelectrocatalytic activity. No bandgap narrowing can be observed from the Tauc plot (**Figure 4b**), indicating that the NCDs are only present on the surface without disrupting the crystalline structure of TiO_2, in line with the STEM and XRD results.

PEC measurements were performed on the aforementioned TiO_2 films to investigate the photo-induced charge transfer behaviour. **Figure 4c-f** show the linear sweep voltammetry (LSV) of the photoelectrodes under simulated solar light irradiation (electrolyte: 0.2 M Na_2SO_4 aqueous solution; scan rate: 5 mV/s). Clearly, the NCDs/TiO_2 photoanode showed enhanced photo-response compared to pure TiO_2; the NCDs/TiO_2 displays a saturation photocurrent of 0.15 mA cm^{-2} at 0.3V vs RHE, approximately two times higher than that of the pristine TiO_2 (0.08 mA cm^{-2}) under the same conditions. This may be the effect of the formation of heterojunctions at the NCDs/TiO_2 interface, which can effectively separate the photo-induced charge carriers. The

expected PEC results under visible light ($\lambda > 420$ nm) further depict the enhanced charge separation of TiO_2 by hybridising NCDs. While TiO_2 electrode showed no obvious photo-response in this region, the NCDs/TiO_2 generated photocurrent of 17 μA cm^{-2}, owing to the slightly enhanced visible absorption of NCDs. Consequently, based on the above results, the photosensitization effect of NCDs on the photocurrent generation of NCDs/TiO_2 heterostructures was unambiguously ascertained under both simulated solar and visible light illuminations.

The distribution of the photocurrent between UV and visible light is given in **Figure S8**. Nearly half of the enhanced photo-carrier generation of NCDs/TiO_2 is attributed to the higher visible light absorption, due to the photosensitization ability of NCDs. The rest of the improved photocurrent may arise from a more efficient charge separation and transportation because of the formed heterojunction between TiO_2 and NCDs.[29,53] Stability test was performed on the NCDs/TiO_2 photoelectrode. As seen from **Figure S9**, NCDs/TiO_2 exhibit a current density decrease in the first 2000s, but with time proceeds, the electrode became more stable, with less than 25 % current density drop. Future work is needed to improve the stability of this hybridized material.

The electron-hole pair separation efficiency were further analysed with EIS measurements. In the Nyquist plots, the charge transfer process at the electrode/electrolyte interface is represented by the diameter of the semicircle at low frequency; a smaller diameter indicates a lower charge transfer resistance. **Figure 4g** shows the Nyquist plots of the TiO_2 and NCDs/TiO_2 photoanodes from 100 kHz to 0.1 Hz under simulated solar light illumination (0.3V vs RHE). The prepared NCDs/TiO_2 show a smaller semi-circular diameter compare to TiO_2 under light illumination, revealing that the NCDs/TiO_2 electrode possesses less photo-induced charge transfer resistance in the interface of electrode and electrolyte, highlighting the key benefit of NCDs in improving charge separation efficiency and enhancing photoelectrochemical activity. Compare with the EIS

performed under dark conditions, we can tell that the charge transfer resistance of NCDs/TiO_2 electrode decreased faster by light illumination compared with pristine TiO_2. This proves that NCDs provided photosensitised electrons to TiO_2 and separated the electron-hole pairs more efficiently, thereby decreasing the impedance under light.[54] Additionally, the Mott-Schottky (M-S) measured at 10 kHz reveals a higher carrier density after NCDs deposition (**Figure 4h**) from the smaller slope of NCDs/TiO_2 curve.[50,55] To minimise the effect of surface state capacitance and the double-layer capacitance at the electrode/electrolyte interface, the frequency of the M-S measurements was chosen to be fast enough to limit the effective filling and unfilling of the electrodes' surface state, as well as restrain the builiding up of double layer capacitance. On that note, even though this analysis is derived from an ideal planar electrode model, the calculation of carrier density for a relative comparison is still reasonable.[56] Measurements at different frequency (1 kHz and 3 kHz) can be found in **Figure S10**. The carrier density (N_D) can be estimated by the equation:

$$\frac{1}{C^2} = \frac{2}{\varepsilon\,\varepsilon_0 A^2 e N_D}\left(V - V_{fb} - \frac{k_B T}{e}\right)$$

Where $e = 1.6 \times 10^{-19}\,C$, $\varepsilon_0 = 8.86 \times 10^{-12}\,F\,m^{-1}$, ε = 55 for (101) facet anatase TiO_2 with a small amount of rutile,[55,57] and C is the capacitance. By using these values, we obtain the average donor densities of $8.44 \times 10^{18}\,cm^{-3}$ and $2.67 \times 10^{19}\,cm^{-3}$ for TiO_2 and NCDs/TiO_2 electrodes, respectively. The extrapolation of the M-S plot to the x- intercept gives flat potential of the electrode, in which the NCDs modified TiO_2 show a slightly negative potential than that of TiO_2, by 0.1 V, which may due to the hybridised band structure of NCDs and TiO_2 and favours the migration of photoinduced electrons from NCDs to TiO_2.[39]

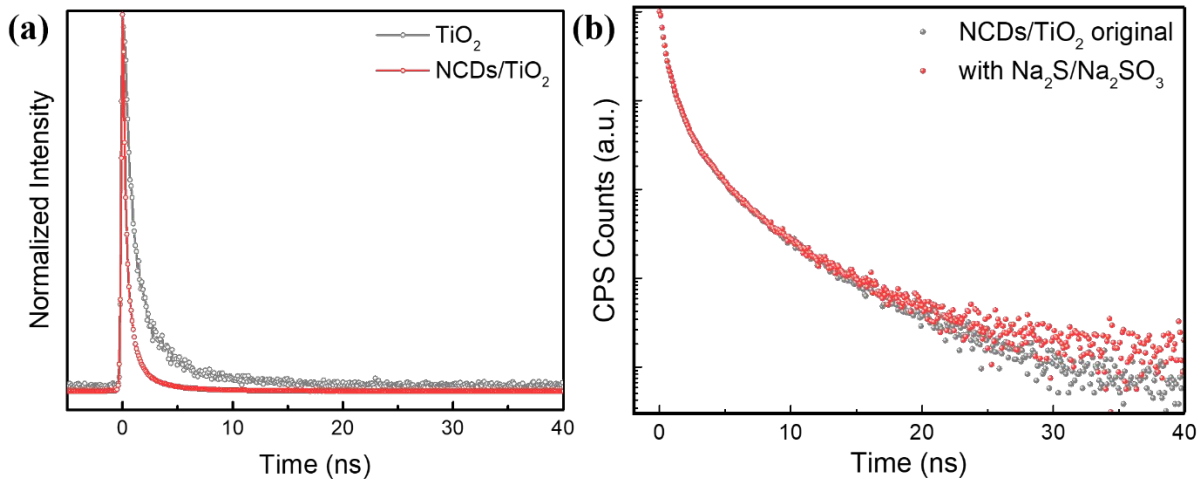

Figure 5 (a) TCSPC decay profile of TiO_2 (grey) and NCDs/TiO_2 (red); (b) decay profiles of NCDs/TiO_2 with (red) and without (grey)the presence of hole scavenger Na_2S/Na_2SO_3. The excitation wavelength for all the experiments is 405 nm, and the emission is recorded at 520 nm.

To further study and gain greater insight into the charge transfer properties in NCDs/TiO_2 heterostructure, Time-correlated Single Photon Counting measurement was performed on pristine TiO_2 and NCDs decorated sample. From **Figure 5a** we can observe a faster photoluminescence (PL) decay after depositing NCDs, which clearly indicate the existence of charge transfer between NCDs and TiO_2, suppressing the radiative charge recombination in TiO_2.[43] The PL quenching of the samples were tested in-situ in an electrolyte with the presence of hole scavengers (Na_2S/Na_2SO_3). It is advised that the presence of hole scavengers can effectively react with photogenerated holes and enrich the electrons in a photocatalyst system,[58] facilitate charge separation and prevent electron-hole recombination, leading to a lower PL and shorter PL lifetime. Comparing the decay profiles of NCDs/TiO_2 with/without hole scavengers in **Figure 5b**, it can be seen that the PL lifetime remained almost identical, suggesting a negligible PL quenching process. In comparison, the PL lifetime of TiO_2 has dramatically decreased from 3.14 ns to 1.75 ns after adding hole scavengers (**Figure S11**). This is probably due to the efficient charge separation in the

NCDs/TiO_2 system, with photogenerated electrons transferred to TiO_2 and holes transported to the surface of NCDs.[59,60]

Combined ultraviolet photoemission spectroscopy (UPS) and photoelectron spectroscopy in air (PESA) techniques provide insights into the electronic structure and energy band positions of the NCDs/TiO_2 materials. The value of ionisation potential of NCD powders from PESA in **Figure S12a** was determined to be 5.5 eV ± 0.02 eV, corresponding to the energy of the highest occupied electronic state (HOMO) of NCDs. The Fermi level of NCDs (E_{f1}) was probed directly by Kelvin probe and was determined to be -4.3 eV. The UV/Vis absorption spectrum of NCDs in **Figure S2a** suggests a relatively large energy gap of 3.5 eV, leaving the lowest unoccupied electronic state (LUMO) at -2 eV. However, the excitation-dependent PL of NCDs (**Figure S2b**) indicates individual energy states of NCDs, which allows energy transitions extending up to 500 nm (2.48 eV).[31] The valence band edge and Fermi level (E_{f2}) of TiO_2 from UPS are -7.65 eV and -5.22 eV, respectively (**Figure S12b**), similar to the reported band position of anatase phase TiO_2.[61,62] The band gap (Eg) was calculated to be 3.21 eV from Tauc plot (**Figure 4b**), from which according to $Eg = E_C - E_V$, the conduction band (CB) edge is estimated to be -4.44 eV, above the H^+/H_2 reduction potential. As to the NCDs/TiO_2, the measured Fermi level (E_{f3}) is -5.16 eV by UPS, in between that of NCDs and TiO_2, consistent with the observation in the PEC Mott-Schottky measurements mentioned previously. A continuous distribution of valence band states is observed up to ~3.6 eV in UPS concerning the Fermi level, indicating there are mid-states existing within the bandgap of the nanocomposite. These states are likely formed at the NCDs/TiO_2 interface and will promote hole transport from the valence band of TiO_2 to the HOMO band of NCDs.[63] Moreover, the ionization energy of NCDs at 5.5 eV, much smaller than the energy for TiO_2 (7.65 eV), clear suggests a transfer of holes from TiO_2 to NCDs.[63] To the best of our knowledge this is

the first report that directly probes the band positions of carbon dots-TiO_2 photoelectrode in a PEC system for understanding the energy transfer mechanism.

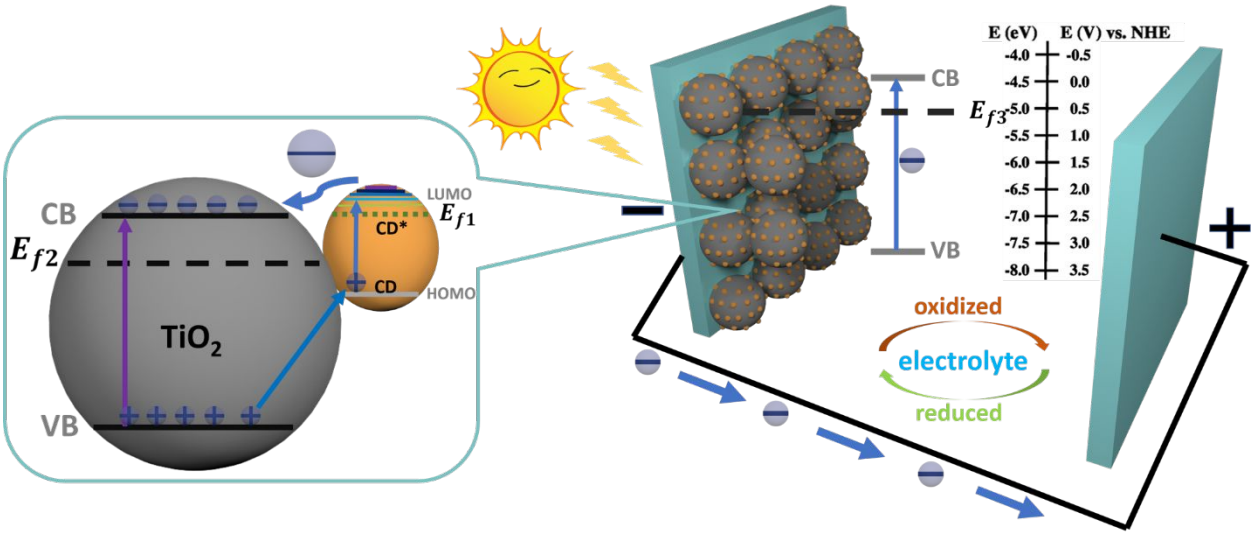

Figure 6 Proposed formation of the heterostructure with band alignments and charge transfer at the surface of TiO_2 and NCDs under light irradiation.

Based on the above results, a schematic diagram of the PEC mechanism is depicted in **Figure 6**. Under full spectrum irradiation, the electrons on the HOMO of NCDs and valence band (VB) of TiO_2 can be effectively excited to the LUMO/CB, respectively. The electrons from the LUMO band of NCDs can then quickly transfer to the CB of the TiO_2 due to its deeper energy level. The holes left in the VB of TiO_2 then transfer to the NCDs, where it can react with the electrolyte for oxidation reactions. The accumulated electrons in TiO_2 would then go into the external circuit to the counter electrode where reduction reactions take place, resulting in a higher measured photocurrent. While under visible light irradiation, the higher photoactivity is induced by obtaining a new absorption band through interfacial charge transfer.[44] Electrons in NCDs were excited from HOMO band on to LUMO band, where they are effectively transferred through TiO2 into the circuit under positive bias, resulted in a higher photocurrent response.

Our work has therefore shown that in this hybrid system the energy levels are arranged such that, a photon excites an electron-hole pair on the NCDs with a subsequent electron transfer to the TiO_2, which would then be transferred to counter electrode. This leaves a hole in the valence band of the NCDs residing at -5.5 eV which provides a site for electron transfer from OH^-, which is the electron donor (D) in the electrolyte solution. The conversion of D^+ from D with NCDs/TiO_2 as photocatalysts under illumination produces the photocurrent, completing the PEC circuit.

3.Conclusions

In summary, a facile solvothermal method was employed to synthesise nanoscale NCDs with good optical and PEC response in the UV-visible range. This type of carbon dots can be applied as a photosensitizer for improving the PEC activity of TiO_2 and used as a model system to understand the fundamental mechanism of sensitisation using NCDs. The obtained NCDs/TiO_2 electrode exhibits a higher photocurrent compared to the pristine TiO_2, with an even greater enhancement under visible light illumination. A variety of complementary techniques such as HR-STEM, EELS, UV-Vis absorption, EIS, M-S, TCSPC and UPS were performed to investigate the optoelectronic properties, photo-induced charge transfer and band structure of the hybrid. The results reveal that the improved PEC activity for the NCDs/TiO_2 arises from the synergistic effect of NCDs combined with TiO_2, which expand the light response into visible range as well as form type II heterojunction at the interface with well-resolved band postion probing which have been reported for the first time. We show here the charge transfer process between NCDs and TiO_2, with in-depth analysis of the energy transitions to develop a comprehensive fundamental understanding on the favoured role of NCDs in the photoelectrocatalytic reactions. The importance of combining structural, photophysical and electrochemical assays on systematically improve the charge transfer process between carbon dots and their catalyst counterparts is also addressed here.

Future work will focus on tuning the carbon dots properties and optimising the hybridisation with other photoelectrocatalytic systems or z-schemes for enhanced photocatalytic performances.

ASSOCIATED CONTENT

Supporting Information

The supporting Information is available free of charge on the ACS Publications website.

More characterizations on NCDs/TiO_2's morphology and chemical/physical properties. (PDF)

AUTHOR INFORMATION

Corresponding Author

*E-mail: m.titirici@imperial.ac.uk

Author Contributions

The manuscript was written through contributions of all authors. All authors have given approval to the final version of the manuscript. HL produced the NCDs/TiO_2 materials and performed all the basic characteristic techniques; SD helped with the TAS and TCSPC measurements; MD, JSK measured the fermi level while MAS, PS and OF helped with UPS and PESA analysis; HL, QG, YF, ABJ, XW and MMT co-wrote the paper. All authors have contributed to revise the manuscript.

Notes

The authors declare no competing financial interest.

ACKNOWLEDGMENT

HL and QG thanks the Chinese government for the award of CSC scholarships, and Dr Enrico Salvadori for the EPR measurement. SD is grateful for financial support by Edinburgh Instruments. This work is part-funded by the European Regional Development Fund through the Welsh Government. We thank the Diamond Light Source for access and support in the use of the electron

Physical Science Imaging Centre (Instrument E01 proposal MG22447) that contributed to the results presented here. PS acknowledges financial support from the Agence Nationale de la Recherche through the Labex projects CSC (ANR-10-LABX-0026 CSC) within the Investissement d'avenir program (ANR-10-120 IDEX-0002-02), by the International Center for Frontier Research in Chemistry (icFRC). OF acknowledges support from the Royal Society through a University Research Fellowship (UF140372). XW thanks the National Natural Science Foundation of China (21861130353).

REFERENCES

(1) Fujishima, A., & Honda, K. Electrochemical Photolysis of Water One and Two-Dimensional Structure of Poly (L-Alanine) Shown by Specific Heat Measurements at Low. *Nature* **1972**, *238*, 37–38.

(2) Zhao, L.; Chen, X.; Wang, X.; Zhang, Y.; Wei, W.; Sun, Y.; Antonietti, M.; Titirici, M. M. One-Step Solvothermal Synthesis of a Carbon @TiO2 Dyade Structure Effectively Promoting Visible-Light Photocatalysis. *Adv. Mater.* **2010**, *22* (30), 3317–3321.

(3) Yoo, I. han; Kalanur, S. S.; Seo, H. A Nanoscale p–n Junction Photoelectrode Consisting of an NiO x Layer on a TiO 2 /CdS Nanorod Core-Shell Structure for Highly Efficient Solar Water Splitting. *Appl. Catal. B Environ.* **2019**, *250* (February), 200–212.

(4) Tada, H.; Mitsui, T.; Kiyonaga, T.; Akita, T.; Tanaka, K. All-Solid-State Z-Scheme in CdS–Au–TiO2 Three-Component Nanojunction System. *Nat. Mater.* **2006**, *5* (10), 782–786.

(5) Zhao, H.; Hu, Z.; Liu, J.; Li, Y.; Wu, M.; Van Tendeloo, G.; Su, B. L. Blue-Edge Slow Photons Promoting Visible-Light Hydrogen Production on Gradient Ternary 3DOM TiO2-Au-CdS Photonic Crystals. *Nano Energy* **2018**, *47* (December 2017), 266–274.

(6) Sant, P. A.; Kamat, P. V. Interparticle Electron Transfer between Size-Quantized CdS and TiO2 Semiconductor Nanoclusters. *Phys. Chem. Chem. Phys.* **2002**, *4* (2), 198–203.

(7) Lee, Y.-L.; Chi, C.-F.; Liau, S.-Y. CdS/CdSe Co-Sensitized TiO2 Photoelectrode for Efficient Hydrogen Generation in a Photoelectrochemical Cell. *Chem. Mater.* **2010**, *22* (3), 922–927.

(8) Zhang, F.; Zhang, C.-L.; Wang, W.-N.; Cong, H.-P.; Qian, H.-S. Titanium Dioxide/Upconversion Nanoparticles/Cadmium Sulfide Nanofibers Enable Enhanced Full-Spectrum Absorption for Superior Solar Light Driven Photocatalysis. *ChemSusChem* **2016**, *9* (12), 1449–1454.

(9) Xiong, Z.; Luo, Y.; Zhao, Y.; Zhang, J.; Zheng, C.; Wu, J. C. S. Synthesis, Characterization and Enhanced Photocatalytic CO2 Reduction Activity of Graphene Supported TiO2 Nanocrystals with Coexposed {001} and {101} Facets. *Phys. Chem. Chem. Phys.* **2016**, *18* (19), 13186–13195.

(10) Lu, Y.; Cheng, X.; Tian, G.; Zhao, H.; He, L.; Hu, J.; Wu, S. M.; Dong, Y.; Chang, G. G.; Lenaerts, S.; Siffert, S.; Van Tendeloo, G.; Li, Z. F.; Xu, L. L.; Yang, X. Y.; Su, B. L. Hierarchical CdS/m-TiO2/G Ternary Photocatalyst for Highly Active Visible Light-Induced Hydrogen Production from Water Splitting with High Stability. *Nano Energy* **2018**, *47* (September 2017), 8–17.

(11) Yu, H.; Zhao, Y.; Zhou, C.; Shang, L.; Peng, Y.; Cao, Y.; Wu, L.-Z.; Tung, C.-H.; Zhang, T. Carbon Quantum Dots/TiO2 Composites for Efficient Photocatalytic Hydrogen Evolution. *J. Mater. Chem. A* **2014**, *2* (10), 3344.

(12) Tian, J.; Leng, Y.; Zhao, Z.; Xia, Y.; Sang, Y.; Hao, P.; Zhan, J.; Li, M.; Liu, H. Carbon Quantum Dots/Hydrogenated TiO2 Nanobelt Heterostructures and Their Broad Spectrum Photocatalytic Properties under UV, Visible, and near-Infrared Irradiation. *Nano Energy* **2015**, *11*, 419–427.

(13) Chen, P.; Wang, F.; Chen, Z. F.; Zhang, Q.; Su, Y.; Shen, L.; Yao, K.; Liu, Y.; Cai, Z.; Lv, W.; Liu, G. Study on the Photocatalytic Mechanism and Detoxicity of Gemfibrozil by a Sunlight-Driven TiO2/Carbon Dots Photocatalyst: The Significant Roles of Reactive Oxygen Species. *Appl. Catal. B Environ.* **2017**, *204*, 250–259.

(14) Wang, Q.; Huang, J.; Sun, H.; Zhang, K.-Q.; Lai, Y. Uniform Carbon Dots@TiO2 Nanotube Arrays with Full Spectrum Wavelength Light Activation for Efficient Dye Degradation and Overall Water Splitting. *Nanoscale* **2017**, *9*, 16046–16058.

(15) Liang, Z.; Hou, H.; Fang, Z.; Gao, F.; Wang, L.; Chen, D.; Yang, W. Hydrogenated TiO2 Nanorod Arrays Decorated with Carbon Quantum Dots toward Efficient Photoelectrochemical Water Splitting. *ACS Appl. Mater. Interfaces* **2019**, *11* (21), 19167–19175.

(16) Shi, W.; Guo, F.; Zhu, C.; Wang, H.; Li, H.; Huang, H.; Liu, Y.; Kang, Z. Carbon Dots Anchored on Octahedral CoO as a Stable Visible-Light-Responsive Composite Photocatalyst for Overall Water Splitting. *J. Mater. Chem. A* **2017**, *5* (ii), 19800–19807.

(17) Martins, N. C. T.; Ângelo, J.; Girão, A. V.; Trindade, T.; Andrade, L.; Mendes, A. N-Doped Carbon Quantum Dots/TiO2 Composite with Improved Photocatalytic Activity. *Appl. Catal. B Environ.* **2016**, *193*, 67–74.

(18) Wang, B.; Deng, Z.; Fu, X.; Li, Z. MoS2/CQDs Obtained by Photoreduction for Assembly of a Ternary MoS2/CQDs/ZnIn2S4 Nanocomposite for Efficient Photocatalytic Hydrogen Evolution under Visible Light. *J. Mater. Chem. A* **2018**, *6* (40), 19735–19742.

(19) Feng, J.; Liu, G.; Yuan, S.; Ma, Y. Influence of Functional Groups on Water Splitting in Carbon Nanodots and Graphitic Carbon Nitride Composites: A Theoretical Mechanism Study. *Phys. Chem. Chem. Phys.* **2017**, *19*, 4997–5003.

(20) Luo, H.; Papaioannou, N.; Salvadori, E.; Roessler, M. M.; Ploenes, G.; Eck, E. R. H.; Tanase, L. C.; Feng, J.; Sun, Y.; Yang, Y.; Danaie, M.; Belen Jorge, A.; Sapelkin, A.; Durrant, J.; Dimitrov, S. D.; Titirici, M. Manipulating the Optical Properties of Carbon Dots by Fine-Tuning Their Structural Features. *ChemSusChem* **2019**, *12* (19), 4335–4335.

(21) Shi, R.; Li, Z.; Yu, H.; Shang, L.; Zhou, C.; Waterhouse, G. I. N.; Wu, L. Z.; Zhang, T. Effect of Nitrogen Doping Level on the Performance of N-Doped Carbon Quantum Dot/TiO2 Composites for Photocatalytic Hydrogen Evolution. *ChemSusChem* **2017**, *10* (22), 4650–4656.

(22) Yan, M.; Hua, Y.; Zhu, F.; Gu, W.; Jiang, J.; Shen, H.; Shi, W. Fabrication of Nitrogen Doped Graphene Quantum Dots-BiOI/MnNb 2 O 6 p-n Junction Photocatalysts with Enhanced Visible Light Efficiency in Photocatalytic Degradation of Antibiotics. *Appl. Catal. B Environ.* **2017**, *202*, 518–527.

(23) Sk, M. A.; Ananthanarayanan, A.; Huang, L.; Lim, K. H.; Chen, P. Revealing the Tunable Photoluminescence Properties of Graphene Quantum Dots. *J. Mater. Chem. C* **2014**, *2* (34), 6954–6960.

(24) Otyepka, M.; Kalytchuk, S.; Rogach, A. L.; Zbořil, R.; Sudolská, M.; Nachtigallová, D.; Holá, K. Graphitic Nitrogen Triggers Red Fluorescence in Carbon Dots. *ACS Nano* **2017**, *11* (12), 12402–12410.

(25) Zhang, Y. Q.; Ma, D. K.; Zhang, Y. G.; Chen, W.; Huang, S. M. N-Doped Carbon Quantum Dots for TiO2-Based Photocatalysts and Dye-Sensitized Solar Cells. *Nano Energy* **2013**, *2* (5), 545–552.

(26) Liang, Z.; Hou, H.; Fang, Z.; Gao, F.; Wang, L.; Chen, D.; Yang, W. Hydrogenated TiO 2 Nanorod Arrays Decorated with Carbon Quantum Dots toward Efficient Photoelectrochemical Water Splitting. *ACS Appl. Mater. Interfaces* **2019**, *11* (21), 19167–19175.

(27) Martindale, B. C. M.; Hutton, G. A. M.; Caputo, C. A.; Prantl, S.; Godin, R.; Durrant, J. R.; Reisner, E. Enhancing Light Absorption and Charge Transfer Efficiency in Carbon Dots through Graphitization and Core Nitrogen Doping. *Angew. Chemie - Int. Ed.* **2017**, *56*, 6459–6463.

(28) Hu, R.; Li, L.; Jin, W. J. Controlling Speciation of Nitrogen in Nitrogen-Doped Carbon Dots by Ferric Ion Catalysis for Enhancing Fluorescence. *Carbon N. Y.* **2017**, *111*, 133–141.

(29) Xie, S.; Su, H.; Wei, W.; Li, M.; Tong, Y.; Mao, Z. Remarkable Photoelectrochemical Performance of Carbon Dots Sensitized TiO $_2$ under Visible Light Irradiation. *J. Mater. Chem. A* **2014**, *2* (39), 16365–16368.

(30) Yang, Y.; Cui, J.; Zheng, M.; Hu, C.; Tan, S.; Xiao, Y.; Yang, Q.; Liu, Y. One-Step Synthesis of Amino-Functionalized Fluorescent Carbon Nanoparticles by Hydrothermal

Carbonization of Chitosan. *Chem. Commun.* **2012**, *48*, 380–382.

(31) Zhang, D.-W.; Papaioannou, N.; David, N. M.; Luo, H.; Gao, H.; Tanase, L. C.; Degousée, T.; Samorì, P.; Sapelkin, A.; Fenwick, O.; Titirici, M.-M.; Krause, S. Photoelectrochemical Response of Carbon Dots (CDs) Derived from Chitosan and Their Use in Electrochemical Imaging. *Mater. Horizons* **2018**, *5*, 423–428.

(32) Marinovic, A.; Kiat, L. S.; Dunn, S.; Titirici, M. M.; Briscoe, J. Carbon-Nanodot Solar Cells from Renewable Precursors. *ChemSusChem* **2017**, *10* (5), 1004–1013.

(33) Shu, C.-K. Degradation Products Formed from Glucosamine in Water. *J. Agric. Food Chem.* **1998**, *46* (3), 1129–1131.

(34) Ortega-Liebana, M. C.; Chung, N. X.; Limpens, R.; Gomez, L.; Hueso, J. L.; Santamaria, J.; Gregorkiewicz, T. Uniform Luminescent Carbon Nanodots Prepared by Rapid Pyrolysis of Organic Precursors Confined within Nanoporous Templating Structures. *Carbon N. Y.* **2017**, *117*, 437–446.

(35) Yang, M.; Li, B.; Zhong, K.; Lu, Y. Photoluminescence Properties of N-Doped Carbon Dots Prepared in Different Solvents and Applications in PH Sensing. *J. Mater. Sci.* **2018**, *53*, 2424–2433.

(36) Santos, C. I. M.; Mariz, I. F. A.; Pinto, S. N.; Gonçalves, G.; Bdikin, I.; Marques, P. A. A. P.; Neves, M. G. P. M. S.; Martinho, J. M. G.; Maçôas, E. M. S. Selective Two-Photon Absorption in Carbon Dots: A Piece of the Photoluminescence Emission Puzzle. *Nanoscale* **2018**, *10* (26), 12505–12514.

(37) Strauss, V.; Margraf, J. T.; Dolle, C.; Butz, B.; Nacken, T. J.; Bauer, W.; Peukert, W.;

Spiecker, E.; Clark, T.; Guldi, D. M. Carbon Nanodots – Towards a Comprehensive Understanding of Their Photoluminescence. *J. Am. Chem. Soc.* **2014**, *49*, 17308–17316.

(38) Sudolská, M.; Dubecký, M.; Sarkar, S.; Reckmeier, C. J.; Zbořil, R.; Rogach, A. L.; Otyepka, M. Nature of Absorption Bands in Oxygen-Functionalized Graphitic Carbon Dots. *J. Phys. Chem. C* **2015**, *119*, 13369–13373.

(39) Li, Y.; Li, P.; Wang, J.; Yang, Y.; Yao, W.; Wei, Z.; Wu, J.; Yan, X.; Xu, X.; Liu, Y.; Zhu, Y. Water Soluble Graphitic Carbon Nitride with Tunable Fluorescence for Boosting Broad-Response Photocatalysis. *Appl. Catal. B Environ.* **2018**, *225* (November 2017), 519–529.

(40) Sahu, S.; Behera, B.; Maiti, T. K.; Mohapatra, S. Simple One-Step Synthesis of Highly Luminescent Carbon Dots from Orange Juice: Application as Excellent Bio-Imaging Agents. *Chem. Commun.* **2012**, *48*, 8835–8837.

(41) Guin, J. P.; Guin, S. K.; Debnath, T.; Ghosh, H. N. Chemically Clean Single-Step Oxido-Reductive Synthesis of Green Luminescent Graphene Quantum Dots as Impending Electrocatalyst. *Carbon N. Y.* **2016**, *109*, 517–528.

(42) Shi, X. F.; Xia, X. Y.; Cui, G. W.; Deng, N.; Zhao, Y. Q.; Zhuo, L. H.; Tang, B. Multiple Exciton Generation Application of PbS Quantum Dots in ZnO@PbS/Graphene Oxide for Enhanced Photocatalytic Activity. *Appl. Catal. B Environ.* **2015**, *163*, 123–128.

(43) Shi, X.; Kim, S.; Fujitsuka, M.; Majima, T. In Situ Observation of NiS Nanoparticles Depositing on Single TiO2 Mesocrystal for Enhanced Photocatalytic Hydrogen Evolution Activity. *Appl. Catal. B Environ.* **2019**.

(44) Lee, K.; Yoon, H.; Ahn, C.; Park, J.; Jeon, S. Strategies to Improve the Photocatalytic

Activity of TiO 2 : 3D Nanostructuring and Heterostructuring with Graphitic Carbon Nanomaterials. *Nanoscale* **2019**, *11* (15), 7025–7040.

(45) Chen, Z.; Dinh, H. N.; Miller, E. *Photoelectrochemical Water Splitting: Standards, Experimental Methods, and Protocols*; Springer, 2013.

(46) Wang, H.; An, T.; Selloni, A. Effect of Reducible Oxide-Metal Cluster Charge Transfer on the Structure and Reactivity of Adsorbed Au and Pt Atoms and Clusters on Anatase TiO2. *J. Chem. Phys.* **2017**, *146* (18), 184703.

(47) Nie, Y. C.; Yu, F.; Wang, L. C.; Xing, Q. J.; Liu, X.; Pei, Y.; Zou, J. P.; Dai, W. L.; Li, Y.; Suib, S. L. Photocatalytic Degradation of Organic Pollutants Coupled with Simultaneous Photocatalytic H2 Evolution over Graphene Quantum Dots/Mn-N-TiO2/g-C3N4 Composite Catalysts: Performance and Mechanism. *Appl. Catal. B Environ.* **2018**, *227* (October 2017), 312–321.

(48) Tian, J.; Leng, Y.; Zhao, Z.; Xia, Y.; Sang, Y.; Hao, P.; Zhan, J.; Li, M.; Liu, H. Carbon Quantum Dots/Hydrogenated TiO2nanobelt Heterostructures and Their Broad Spectrum Photocatalytic Properties under UV, Visible, and near-Infrared Irradiation. *Nano Energy* **2015**, *11*, 419–427.

(49) Yu, L.; Shao, Y.; Li, D. Direct Combination of Hydrogen Evolution from Water and Methane Conversion in a Photocatalytic System over Pt/TiO2. *Appl. Catal. B Environ.* **2017**, *204*, 216–223.

(50) Xu, Y.; Zhang, C.; Zhang, L.; Zhang, X.; Yao, H.; Shi, J. Pd-Catalyzed Instant Hydrogenation of TiO 2 with Enhanced Photocatalytic Performance. *Energy Environ. Sci.*

2016, *9* (7), 2410–2417.

(51) D'Angelo, D.; Bongiorno, C.; Amato, M.; Deretzis, I.; La Magna, A.; Fazio, E.; Scalese, S. Oxygen Functionalities Evolution in Thermally Treated Graphene Oxide Featured by EELS and DFT Calculations. *J. Phys. Chem. C* **2017**, *121* (9), 5408–5414.

(52) Rajender, G.; Kumar, J.; Giri, P. K. Interfacial Charge Transfer in Oxygen Deficient TiO2-Graphene Quantum Dot Hybrid and Its Influence on the Enhanced Visible Light Photocatalysis. *Appl. Catal. B Environ.* **2018**, *224* (October 2017), 960–972.

(53) Raziq, F.; Sun, L.; Wang, Y.; Zhang, X.; Humayun, M.; Ali, S.; Bai, L.; Qu, Y.; Yu, H.; Jing, L. Synthesis of Large Surface-Area g-C3N4 Comodified with MnOx and Au-TiO2 as Efficient Visible-Light Photocatalysts for Fuel Production. *Adv. Energy Mater.* **2018**, *8* (3), 2–11.

(54) Tzeng, W. J.; Wu, M. L.; Lin, L. J.; Chang, H. Y. Chalcogenide Photosensitized Titania Nanotube Arrays. *J. Alloys Compd.* **2015**, *651* (December 2015), 483–489.

(55) Goossens, A.; Schoonman, J. Mott-Schottky Analysis of Nanometer-Scale. *J. Electrochem. Soc.* **1997**, *144* (5), 1723–1727.

(56) Luo, Z.; Wang, T.; Zhang, J.; Li, C.; Li, H.; Gong, J. Dendritic Hematite Nanoarray Photoanode Modified with a Conformal Titanium Dioxide Interlayer for Effective Charge Collection. *Angew. Chemie - Int. Ed.* **2017**, *56* (42), 12878–12882.

(57) Kim, J. Y.; Jung, H. S.; No, J. H.; Kim, J. R.; Hong, K. S. Influence of Anatase-Rutile Phase Transformation on Dielectric Properties of Sol-Gel Derived TiO2 Thin Films. *J. Electroceramics* **2006**, *16* (4), 447–451.

(58) Kudo, A.; Miseki, Y. Heterogeneous Photocatalyst Materials for Water Splitting. *Chem. Soc. Rev.* **2009**, *38* (1), 253–278.

(59) Ma, Z.; Zhang, Y.-L.; Wang, L.; Ming, H.; Li, H.; Zhang, X.; Wang, F.; Liu, Y.; Kang, Z.; Lee, S.-T. Bioinspired Photoelectric Conversion System Based on Carbon-Quantum-Dot-Doped Dye–Semiconductor Complex. *ACS Appl. Mater. Interfaces* **2013**, *5* (11), 5080–5084.

(60) Liu, R.; Huang, H.; Li, H.; Liu, Y.; Zhong, J.; Li, Y.; Zhang, S.; Kang, Z. Metal Nanoparticle / Carbon Quantum Dot Composite as Photocatalyst for High Efficiency Cyclohexane Oxidation. *Acs Catal.* **2014**, *4*, 328–336.

(61) Scanlon, D. O.; Dunnill, C. W.; Buckeridge, J.; Shevlin, S. A.; Logsdail, A. J.; Woodley, S. M.; Catlow, C. R. A.; Powell, M. J.; Palgrave, R. G.; Parkin, I. P.; Watson, G. W.; Keal, T. W.; Sherwood, P.; Walsh, A.; Sokol, A. A. Band Alignment of Rutile and Anatase TiO2. *Nat. Mater.* **2013**, *12* (9), 798–801.

(62) Kashiwaya, S.; Morasch, J.; Streibel, V.; Toupance, T.; Jaegermann, W.; Klein, A. The Work Function of TiO2. *Surfaces* **2018**, *1* (1), 73–89.

(63) Saha, A.; Moya, A.; Kahnt, A.; Iglesias, D.; Marchesan, S.; Wannemacher, R.; Prato, M.; Vilatela, J. J.; Guldi, D. M. Interfacial Charge Transfer in Functionalized Multi-Walled Carbon Nanotube@TiO2 Nanofibres. *Nanoscale* **2017**, *9* (23), 7911–7921.

Table of Contents

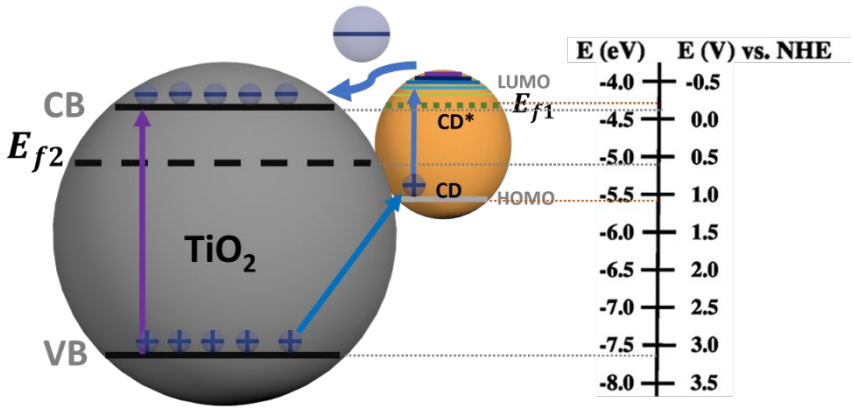

Type II heterojunction with well-resolved band positions

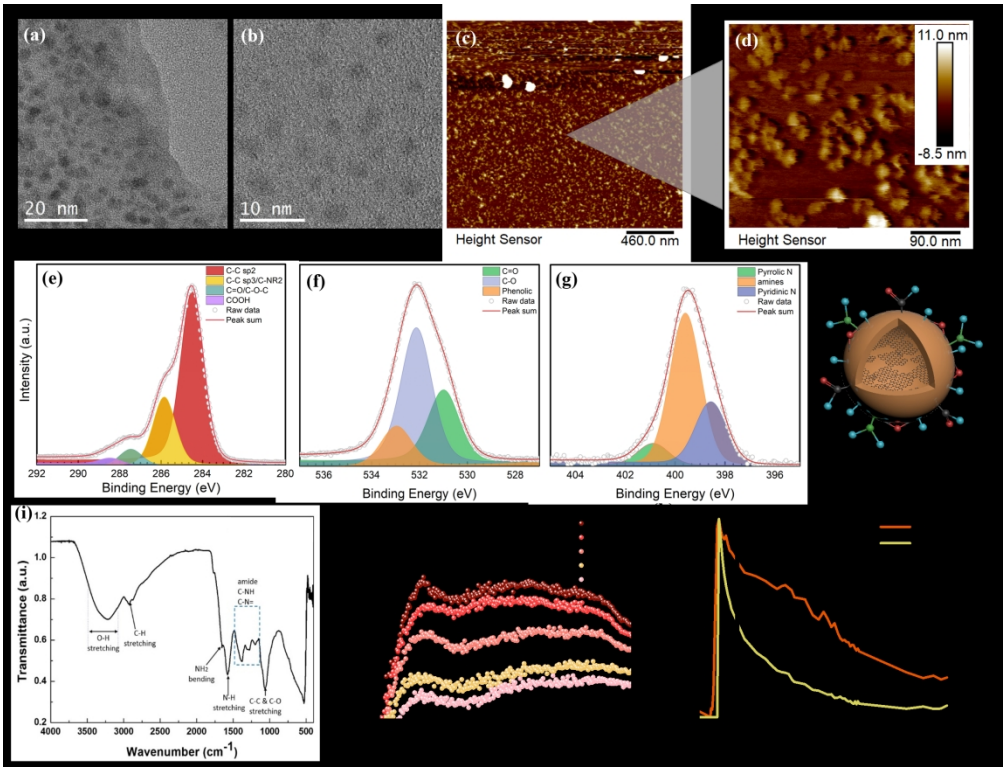

Figure 1 Structural features of as-prepared NCDs: TEM (a) and HR-TEM (b) images; (c) an overview AFM image on mica substrate (Z scale -6.0 to 7.9 nm) and (d) high-resolution scanned image; XPS spectra: (e) C 1s, (f) O 1s, (g) N 1s and corresponding FTIR (i) spectrum; (h) a schematic structure based on the characterizations (atoms in red: O, green: N and blue: H); (j) fs-TAS spectra at different time decays and (k) normalized fs-TAS kinetics of NCDs and non-doped CDs measured at 500 nm, samples were excited at 375 nm.

464x353mm (150 x 150 DPI)

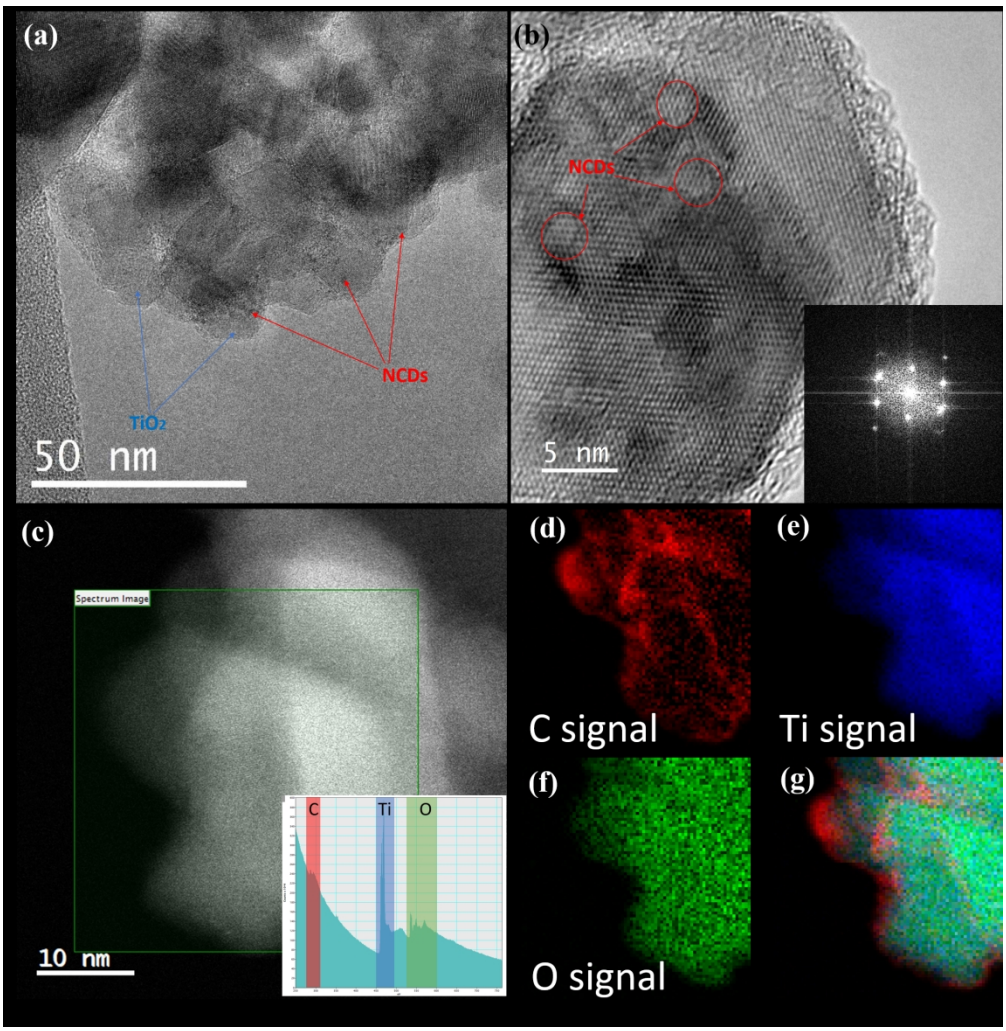

Figure 2 TEM (a) and HR-TEM (b) of NCDs/TiO2 (insert is the FFT patterns); (c) HAADF image of NCDs/TiO2 and corresponding EELS spectra (inserted). The single element maps derived from the spectra: (d) C signal, (e) Ti signal, (f) O signal and (g) colour mix (red: C, blue: Ti, green: O).

373x380mm (150 x 150 DPI)

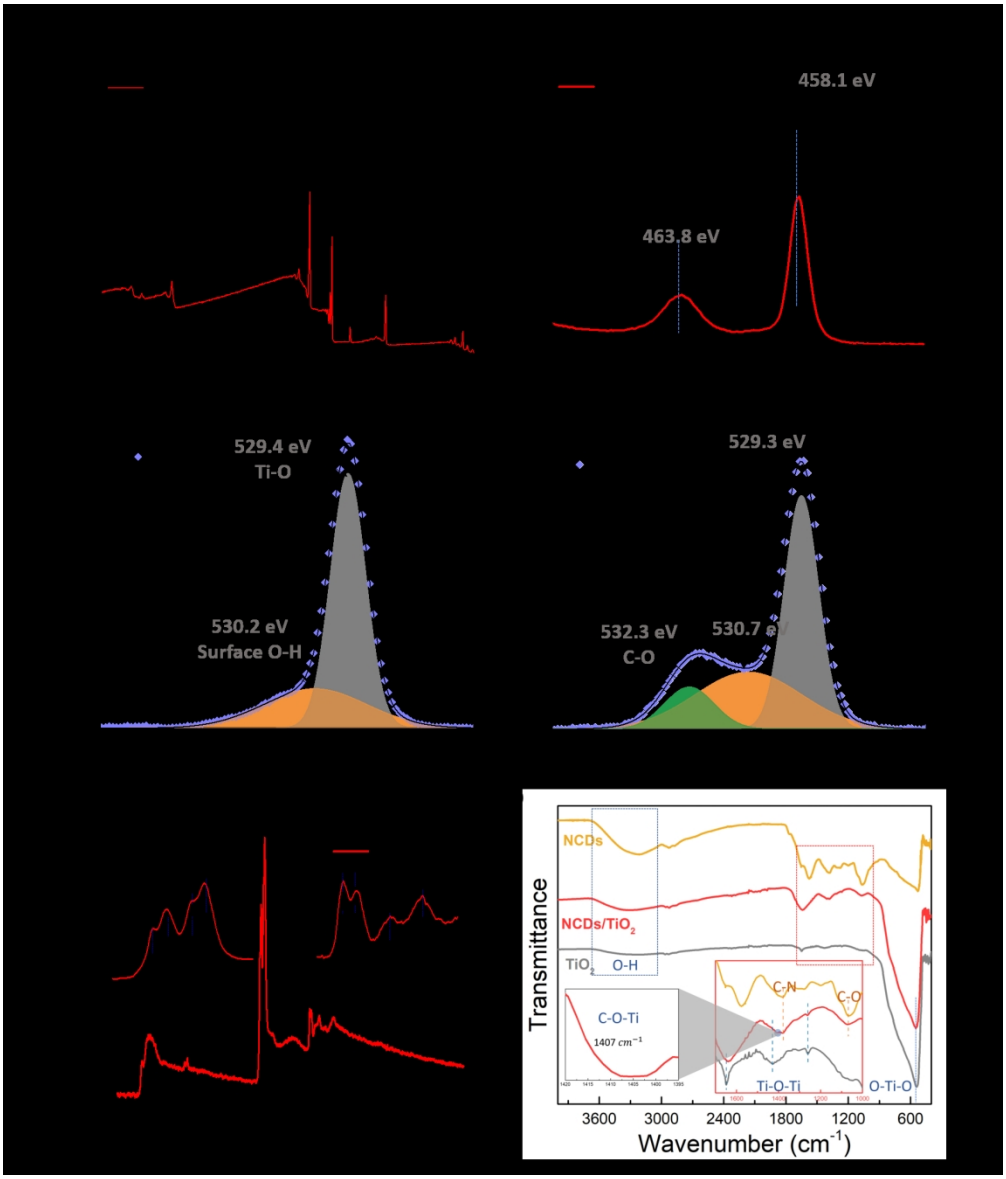

Figure 3 Comparison of XPS survey spectra (a) and corresponding core level spectra (b) Ti 2p of the TiO2 and NCDs/TiO2 films; O 1s spectra of (c) TiO2 and (d) NCDs/TiO2. (e) EELS spectra of TiO2 (black) and NCDs/TiO2 (red) and (f) FTIR signals.

313x366mm (150 x 150 DPI)

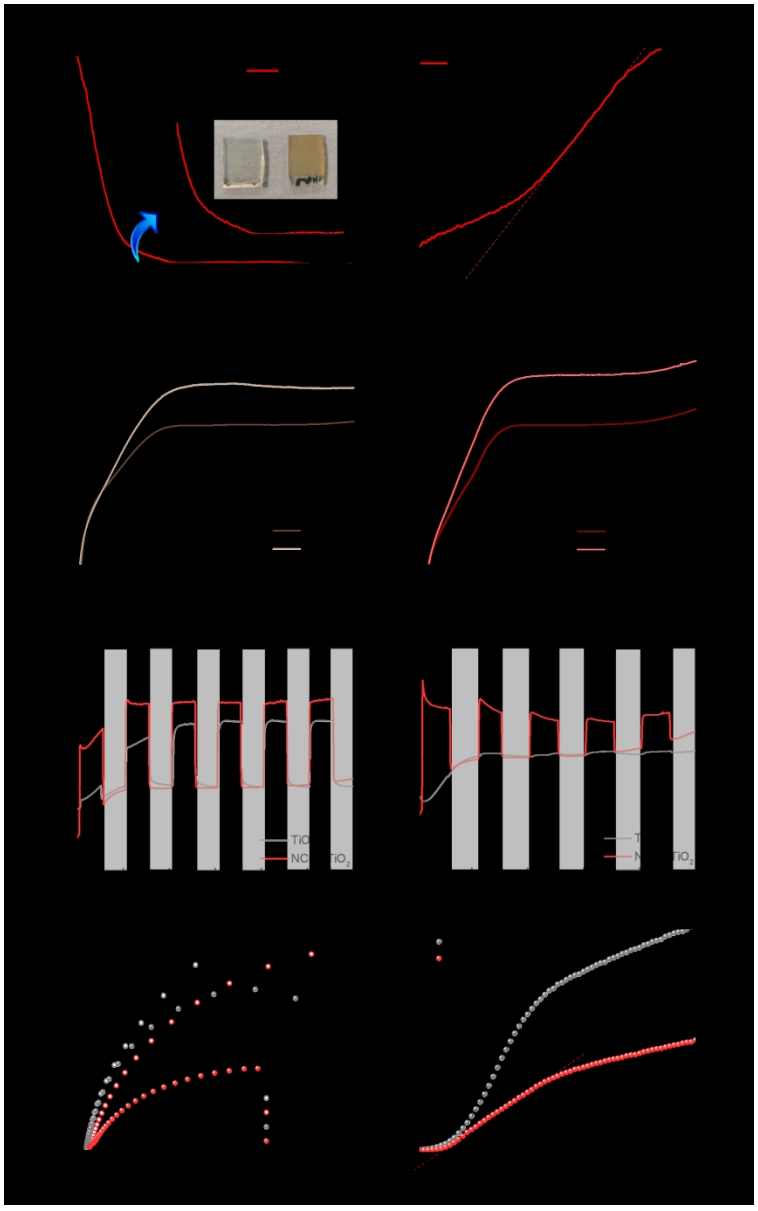

Figure 4 optoelectronic properties of TiO2 and NCDs/TiO2 films: (a) UV-Vis absorption (inserted are the digital pictures of the films: left: TiO2, right: NCDs/TiO2); (b) tauc plot of TiO2 and NCDs/TiO2 with indirect band gap; LSV curves of (c) TiO2 and (d) NCDs/TiO2 under dark and light conditions; the chopped photocurrent response of the two samples under (e) full spectrum and (f) visible light (λ > 420 nm) illumination; (g) EIS Nyquist plots under simulated solar light illumination (100 kHz – 0.1 Hz, 0.3V vs. RHE, 100 mW cm-2) and (h) Mott-Schottky plots with 10 kHz frequency under dark condition at equilibrium.

317x506mm (150 x 150 DPI)

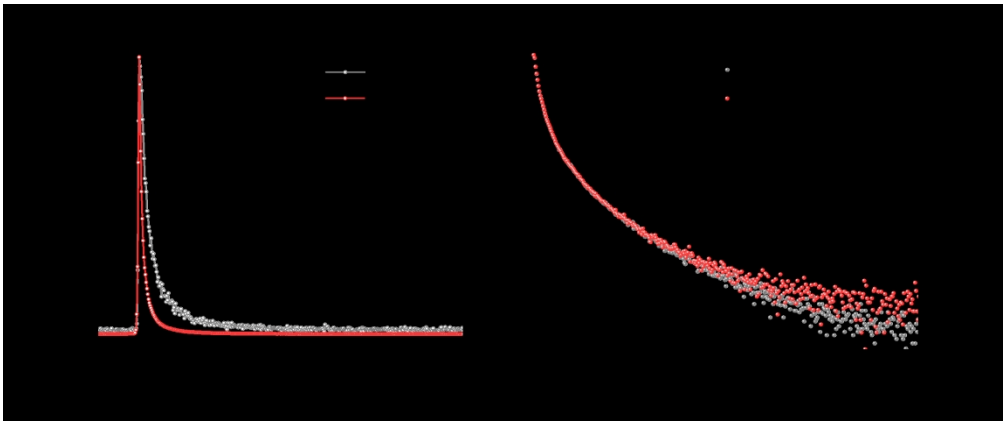

Figure 5 (a) TCSPC decay profile of TiO2 (grey) and NCDs/TiO2 (red); (b) decay profiles of NCDs/TiO2 with (red) and without (grey)the presence of hole scavenger Na2S/Na2SO3. The excitation wavelength for all the experiments is 405 nm, and the emission is recorded at 520 nm.

423x176mm (150 x 150 DPI)

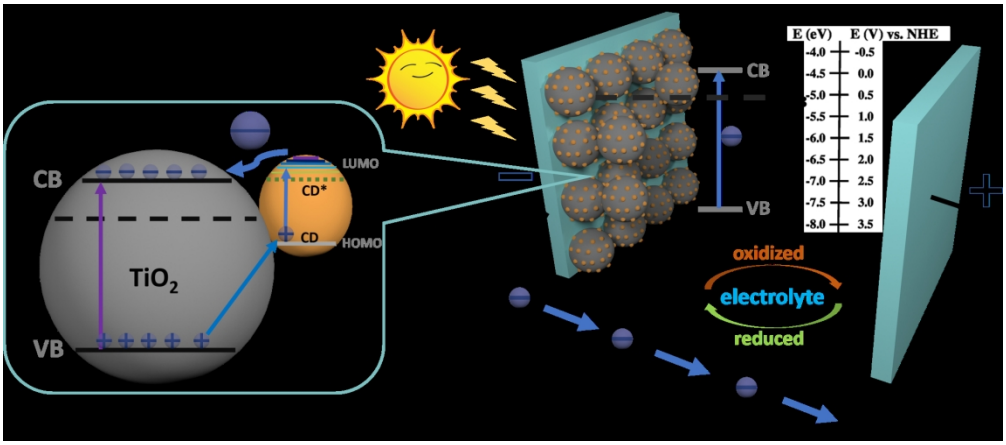

Figure 6 Proposed formation of the heterostructure with band alignments and charge transfer at the surface of TiO2 and NCDs under light irradiation.

353x154mm (150 x 150 DPI)